Mode Identification of Broadband Lamb Wave Signal with Squeezed Wavelet Transform

Shen Wang[1*], Songling Huang[1] Qing Wang[2] Yu Zhang[1] Wei Zhao[1]

[1]State Key Lab. Of Power System, Dept. of Electrical Engineering, Tsinghua University, Beijing 100084, China

[2] School of Engineering and Computing Sciences, Durham University, DH1 3LE Durham, United Kingdom

***Abstract*—** Multiple wave modes often exist in the ultrasonic guided waves simultaneously, and these modes are dispersive, so the guided wave signals are very complex, even for the relatively simple situation of a narrowband excitation. The guided wave signals are even more difficult to analyze for broadband excitations. Time-frequency representations are appropriate for the analysis of the guided wave signals considering their non-stationary and transient nature. As a post-processing tool, the squeezed wavelet transform is studied for broadband Lamb wave mode identification in this work. The influence of the parameters of the Gabor mother wavelet on the performance of the transform is analyzed in detail. It is found that the product of the σ parameter of the used Gauss function and the center frequency ω_0 of the wavelet decides the overall time and frequency resolutions, so a proper selection of the value of this product $\sigma\omega_0$ is crucial for the squeezed wavelet transform. The squeezed wavelet transform is first applied to the analysis of a synthesized signal for verification. Then it's applied for mode identification of a simulated broadband Lamb wave signal. By traversing the value of $\sigma\omega_0$, a roughly optimum analysis performance is achieved for the squeezed wavelet transform for the case of $\sigma\omega_0 = 11$, where the modes are well separated and the interferences between the modes are minimal. It's proved that as an alternative tool, the squeezed wavelet transform could be used for the analysis of a broadband Lamb wave signal. An additional benefit of this transform is that it permits reconstruction of the original signal or its components, which is not possible for the reassigned scalogram.

Keywords— Broadband lamb wave, mode identification, time-frequency representation, analytic wavelet transform, squeezed wavelet transform.

* Corresponding author.
Email address: wangshen@mail.tsinghua.edu.cn (S. Wang)

1. Introduction

Ultrasonic waves propagating along the extension direction of bounded elastic media like the plate and the pipe are called guided waves. Accordingly the structures they propagate in are waveguides. Guided waves are increasingly used in the inspection of various plate-like and pipe-like critical structures in different fields because they can be used to check the whole line along the propagation direction in the structure from one single point, thus reducing the time consumption unavoidable in the traditional bulk wave-based point-by-point ultrasonic inspection.

Despite the advantages, multiple modes often exist in the guided waves, and these modes are dispersive in the sense that the propagating velocities of the wave modes are functions of the frequency. Because of this dispersion phenomenon, the guided waves are more complex than the bulk waves, speaking of their propagations and interactions with the defects. Even when one approximately pure mode is generated with a narrowband excitation, the features of the guided waves might be mixed together in the time domain, thus making the interpretation of the received guided wave signal difficult. If a broadband excitation is applied, the complexity of the signal is even higher. This situation demands an effective analyzing tool for mode identification from the guided wave signals.

Guided wave signals are typical transient and non-stationary signals with time-varying frequency components. The common tool for the analysis of the non-stationary signals is the time-frequency representations (TFRs). Unlike the original unprocessed pure time domain description or the pure frequency domain description provided by the Fourier transform, the TFRs map the signal as a 2D function of both time and frequency. A by-product of the TFR is just what we're most interested in, the evolution of the frequencies of the components contained in the signal with time.

With the TFRs at our disposal and taking into account the distance of propagation of the guided waves, we can convert the theoretical group velocity dispersion curves of the guided waves from the frequency-velocity plane to the time-frequency plane. With this method, we can directly tell what modes are present in the received signal, so it helps greatly with the

interpretation of the guided wave signals. This process was first seen in the work of Prosser et al. [1].

There're mainly two types of TFRs, i.e. the linear TFRs and the bilinear TFRs. In the linear TFRs the signal is projected to a group of time-frequency atoms [2], and the results of the TFRs are the weights of projection on these atoms. The earliest linear TFR is the short-time Fourier transform (STFT), a localized version of the Fourier transform. The STFT and the derived spectrogram are relatively easy to comprehend and are used widely. One problem of this TFR is that with the restriction imposed by the uncertainty principle, one can't obtain arbitrarily high time and frequency resolutions simultaneously. Another problem is that its time and frequency resolutions are fixed, once the window function is selected.

Another popular linear TFR is the continuous wavelet transform (WT), which is in fact a time-scale transform. Roughly speaking, the scale parameter is the reciprocal of the frequency. The timescale atoms of the WT are generated from a mother wavelet, and the atoms form a time-scale dictionary with varying time/translation and scale parameters. At a low frequency (high scale), a longer time window (which means a narrower frequency window) is used, so the WT has lower time resolution and higher frequency resolution. At a high frequency (low scale), a shorter time window (which means a broader frequency window) is used, so the WT has higher time resolution and lower frequency resolution. The automatic adjustment of the resolutions is the main advantage of the WT. As a linear TFR, the WT is also limited by the uncertainty principle, so we can't achieve arbitrarily high time and frequency resolutions simultaneously.

Wavelets were already used in the analysis of ultrasonic guided wave signals. The Mexican Hat wavelet is a real wavelet, and it was used to measure the group velocity of the Lamb waves, so as to obtain the corrosion thickness in the plate [3]. The Mexican Hat wavelet was also used to analyze the signals generated by EMATs to identify the guided wave modes, for the tomography of artificial defects in the plate [4]. Besides the real wavelets, the complex Morlet/Gabor wavelets are often used. The Morlet wavelet was applied for the transient wave analysis in the dispersive media [5], the study of the interactions of the Lamb waves with circumferential notch in an aluminum alloyed pipeline [6], the research on the interactions of the Lamb waves with hidden corrosion defects in the aircraft aluminum structure [7], and the

analysis of the multi-mode guided wave signals in the multi-wire cables [8]. Liu used the Gabor wavelet to analyze the signals of the circumferential guided waves to detect axial cracking in the pipeline [9]. Lee used the Gabor wavelet for the analysis of the signals of the guided waves propagating in the rock bolts [10].

Different from the linear TFRs, the bilinear TFRs directly correspond to the energy distributions, i.e. they map the energy of the signal as a function of time and frequency. The most important bilinear TFR is the Wigner-Ville distribution (WVD). The WVD has perfect concentration for the single component linear chirp signal, while because it has the form of a product followed by integration, cross terms emerge for the analysis of multi-component signals with the WVD. To lower the influences of these cross terms, the complex analytic signal corresponding to the original real signal is generally used in the computation of the WVD, and smoothing is introduced as in the pseudo WVD (PWVD) and the smoothed PWVD (SPWVD), although the smoothing is obtained at the price of lower time-frequency resolutions. The PWVD was used in the dispersion analysis of the Lamb waves propagating in the graphite/epoxy plates [1,11].

With the limitations imposed by the uncertainty principle, the linear TFRs have constrained time-frequency resolutions, while the bilinear TFRs, represented by the WVD, have interferences because of the cross terms. To improve the readability of these TFRs, Auger 'rediscovered' the reassigned time-frequency and time-scale representations [12]. With these reassigned versions of the original TFRs, better time-frequency concentrations are achieved. Niethammer used the reassigned spectrogram to obtain the dispersion curves of laser-generated multiple Lamb wave modes in the aluminum plate [13,14]. The reassigned spectrogram was later used in other applications like locating the defects [15].

Besides the normal TFRs, another tool or algorithm for nonstationary and nonlinear signal analysis is the empirical mode decomposition (EMD) in time domain combined with the Hilbert transform (HT). The EMD method is used to decompose a signal into intrinsic mode functions (IMFs). Then HT is applied to the IMFs to obtain instantaneous frequency data. During the recent years, the EMD and HT method is increasingly used in mode recognition of Lamb waves. Zhang applied the method to analyse both directly arriving and boundary-reflected Lamb wave modes of opposite types (S0 and A0) [16]. The EMD and HT method was also used to extract

arrival times of Lamb waves for imaging applications [17]. This work only used narrow-banded excitations, so we will not explore further the EMD and HT method here.

In this work, an alternative wavelet post-processing technique called squeezing, proposed by Daubechies et al. [18,19], is studied for the analysis of multimode Lamb wave signal. With firstly a review of the common TFRs and the reassignment concept, the selection of the parameters of the mother wavelet is investigated, and then the squeezing theory is introduced. The squeezed wavelet transform is applied first to a synthesized signal, then to the simulated broadband Lamb wave signal. The parameters of the mother wavelet are traversed to obtain a roughly optimum performance. Although the squeezed wavelet transform provides no better performance for the analysis of the broadband Lamb wave signal than the reassigned scalogram, it proves to be an alternative tool and has the additional advantage of permitting reconstruction of the original signal or its components, which is not possible for the reassigned TFRs.

2. Brief review of the time-frequency representations and the reassigned linear representations

2.1 The time-frequency representations

The basic tool for the frequency domain analysis of a signal f (t) is the Fourier transform (FT),

$$F(\omega) = \int_{-\infty}^{+\infty} f(t) \mathrm{e}^{-\mathrm{j}\omega t} \mathrm{d}t \qquad (1)$$

in which ω is the angular frequency in rad/s.

The inverse Fourier transform, or the reconstruction formula from the known Fourier transform coefficients, is

$$f(t) = \frac{1}{2\pi} \int_{-\infty}^{+\infty} F(\omega) \mathrm{e}^{\mathrm{j}\omega t} \mathrm{d}\omega \qquad (2)$$

The time information is completely lost in the Fourier transform (1), and the frequency information is absent from the original time-domain representation as in (2). The Fourier transform is only satisfactory for the representation of stationary signals whose frequency contents don't change with time. While in reality we're more often confronted with non-

stationary signals with time-evolving frequency contents. One example is the recorded music signal, and all the rhythms, beautiful or not, rely on the changing frequency contents. The guided wave signal that we're interested in is another non-stationary signal, considering its dispersive and transient nature. For proper handling of the non-stationary signals, analysis tools other than the Fourier transform are necessary.

One possible solution is the time-frequency representations expressed as two dimensional functions of the time variable t and the frequency variable ω. The first type of the time frequency representations is the linear representations [2]. A prototype function Ø(t) is used to generate a dictionary of waveforms $\mathfrak{D} = \{\emptyset_r(t)\}\gamma\epsilon\Gamma$ in which γ is the index of the waveforms in the dictionary, and possibly has multiple components. The linear TFRs correlate the signal x(t) with the waveforms in $\mathfrak{D}$ as:

$$LIN_x^{\phi}(\gamma) = \langle x(t), \phi_\gamma(t) \rangle \qquad (3)$$

$\langle .,. \rangle$ is the inner product defined as $\langle x(t), y(t) \rangle = \int_{-\infty}^{+\infty} x(t) y*(t) dt$ means complex conjugate.

If we express the time and frequency widths as Δt_γ and $\Delta \omega_\gamma$ respectively, the Heisenberg uncertainty principle states that the area defined by $\Delta t_\gamma \, \Delta \omega_\gamma$ is lower bounded,

$$\Delta t_\gamma \, \Delta \omega_\gamma \geq \frac{1}{2} \qquad (4)$$

The important fact revealed by (4) is that we can't obtain a perfect concentration both in time and in frequency simultaneously for any time-frequency atom Ø(t) generated from the prototype function Ø(t). So for the linear TFRs, the time and the frequency resolutions are limited.

One of the most widely used linear TFRs is the short-time Fourier transform (STFT) defined as,

$$\mathrm{STFT}_x^g(t,\omega) = \langle x(\tau), g_{t,\omega}(\tau) \rangle = \int_{-\infty}^{+\infty} x(\tau) g^*(\tau - t) \mathrm{e}^{-\mathrm{j}\omega\tau} \mathrm{d}\tau \qquad (5)$$

in which g(t) is some window function, and the generated time-frequency atoms have the form of g t,ω (τ) = g(τ-t)$e^{j\omega\tau}$.

The STFT is often used to generate another representation called the spectrogram, defined as,

$$\mathrm{SPEC}_x^g(t,\omega) = \left|\mathrm{STFT}_x^g(t,\omega)\right|^2 = \left|\int_{-\infty}^{+\infty} x(\tau)g^*(\tau - t)\mathrm{e}^{-\mathrm{j}\omega\tau}\,\mathrm{d}\tau\right|^2 \qquad (6)$$

The unavoidable problems of the STFT and the derived spectrogram are the selection of a proper window function g(t) and the selection of the length of this window function. Another problem is that the time width and the frequency width of the timefrequency atoms don't change with the index components t or ω, so they have fixed time and frequency resolutions once the prototype or the window function g(t) and its time length are selected. This characteristic of fixed time and frequency resolutions is often not preferable.

The variable resolution analysis could be implemented by another linear TFR called the wavelet transform, defined using a prototype function (mother wavelet) Ψ(t). The atoms have the form of $\Psi_{u,s}(t) = S^{-\frac{1}{2}}\Psi(\frac{t-u}{s})$ in which t is the independent variable, s is the scale parameter and μ is the translation in time. The wavelet transform applied to the signal x(t) is

$$\mathrm{WT}_x^{\psi}(u,s) = \langle x(\tau), \psi_{u,s}(\tau)\rangle = \frac{1}{\sqrt{s}}\int_{-\infty}^{+\infty} x(\tau)\psi^*\left(\frac{\tau - u}{s}\right)\mathrm{d}\tau \qquad (7)$$

The wavelet transform has the unique advantage over the STFT as it has variable time-frequency resolutions. Roughly speaking, the time-frequency box has a bigger time width and a smaller frequency width (better frequency resolution) at a lower frequency, and has a smaller time width and a bigger frequency width (better time resolution) at a higher frequency.

The wavelet transform is often used to generate a related TFR called the scalogram, as

$$\mathrm{SCAL}_x^{\psi}(u,s) = \left|\mathrm{WT}_x^{\psi}(u,s)\right|^2 = \left|\frac{1}{\sqrt{s}}\int_{-\infty}^{+\infty} x(\tau)\psi^*\left(\frac{\tau - u}{s}\right)\mathrm{d}\tau\right|^2 \qquad (8)$$

Besides the linear TFRs, we also have the bilinear TFRs. The most important bilinear TFR is the Wigner-Ville distribution (WVD) defined as

$$\mathrm{WVD}_x(t,\omega) = \int_{-\infty}^{+\infty} x\left(t + \frac{\tau}{2}\right)x^*\left(t - \frac{\tau}{2}\right)\mathrm{e}^{-\mathrm{j}\omega\tau}\,\mathrm{d}\tau \qquad (9)$$

Without relying on a prototype function, the time and frequency resolutions of the WVD are not limited by the uncertainty principle, and it has many good properties. It can achieve perfect concentration for a single component linear chirp signal, while the disadvantages include that it

has cross terms for signals with multiple frequency components and that this distribution is not always positive so as to invalidate its interpretation as a real energy distribution.

2.2 Concept of time-frequency reassignment

The time-frequency reassignment method is a tool for postprocessing the time-frequency representations. This method improves the readability of the original TFR. The theory starts from an alternative expression of the spectrogram [20],

$$\mathrm{SPEC}_x^g(t,\omega) = \int_{-\infty}^{+\infty}\int_{-\infty}^{+\infty} \mathrm{WVD}_x(\tau,\xi)\mathrm{WVD}_g(\tau - t, \xi - \omega)\mathrm{d}\tau\mathrm{d}\xi \tag{10}$$

in which WVDx(τ, ξ) is the WVD of the signal x(t), and WVDg(τ, ξ) is the WVD of the window function g(t). The spectrogram at the point (t, ω) is thus the average of WVDx(τ, ξ) weighted by WVDg ($\tau - t, \xi - \omega$), in the region of support of WVDg ($\tau - t, \xi - \omega$). WVDg ($\tau - t, \xi - \omega$) is just a time shift t and frequency shift ω version of WVDg(τ, ξ) VDgðs; which is generally concentrated at the origin.

The averaging process from the double integral assigns the result to the geometry center (t, ω) of the region decided by the support of WVDg ($\tau - t, \xi - \omega$). A better solution is to assign the averaging result or the calculated spectrogram value at (t, ω) to the gravity center of the region, and this process is called reassignment. Detailed expressions of the reassignment operators are not given here. Besides the reassigned spectrogram, a similar reassigned algorithm for the scalogram also exists [20].

The time-frequency reassignment method can greatly improve the readability of the TFRs so as to help with the mode identification and separation of the guided wave signals.

3. The analytic wavelet transform and the overall resolutions controlled by the parameters of the mother wavelet

A function f(t) is said to be analytic if it only has positive frequency components [2],

$$F(\omega) = 0, \quad \text{for} \quad \omega < 0 \tag{11}$$

in which F(ω) is the Fourier tranform of f(t).

A complex value wavelet function is called an analytic wavelet, if it's an analytic function, i.e. it satisfies (11). The benefit of using an analytic wavelet is at least that it permits an easy and meaningful conversion between the scale parameters and the pseudo angular frequency ω,

$$\omega = \frac{\omega_c}{s} \tag{12}$$

With ωc as the center angular frequency of the frequency spectrum Ψ(ω) of the mother wavelet Ψ (t). If Ψ(ω) concentrates around ω_c it reaches its maximum at ω_c.

One widely used construction of an analytic wavelet is a window function g(t) modulated with a frequency component $e^{j\omega_0 t}$,

$$\psi(t) = g(t)e^{j\omega_0 t} \tag{13}$$

The Fourier transform of the constructed mother wavelet is Ψ (ω) = G(ω –ω_0), and it's just the frequency shift of G(ω) to a new frequency point ω_0. If G(ω) has a compact support and the frequency shift ω_0 is big enough, we can make sure that Ψ (ω) is almost zero for negative frequencies, thus obtaining an 'almost analytic' mother wavelet.

We obtain a Gabor wavelet if the Gauss function is used as the window function g(t)(13),

$$g(t) = \frac{1}{(\pi\sigma^2)^{\frac{1}{4}}} e^{-\frac{t^2}{2\sigma^2}}, \tag{14}$$

With $\sigma > 0$.

The Fourier transform of g(t) is

$$G(\omega) = (4\pi\sigma^2)^{\frac{1}{4}} e^{-\frac{\sigma^2\omega^2}{2}} \tag{15}$$

Obviously the σ parameter could be used to adjust the time and frequency widths of the Gauss function and hence the Gabor mother wavelet. Now we can draw the waveforms of the Gabor mother wavelet Ψ (t) (real part only) and its Fourier transform Ψ (ω) , as in Fig. 1. Two combinations of σ and ω_0 parameters are used. The first one is σ = 1, ω_0 = 6 and the second one is σ = 2, ω_0 = 4. It could be seen that σ decides the time and frequency spread and ω_0 is just the frequency center.

The Gauss function used in the definition of a Gabor mother wavelet has many good properties and makes it possible to obtain the following simple results.

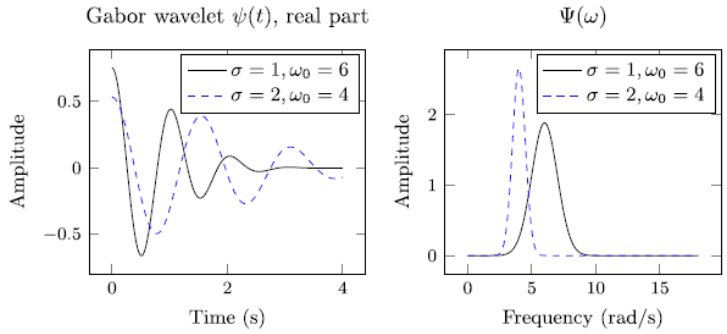

Fig.1 Gabor mother wavelet Ψ (t) (real part) and its Fourier transform Ψ (ω) for σ = 1, ω_0 = 6 and σ = 2, ω_0 = 4.

Firstly, we have an approximate lower bound for $\sigma\ \omega_0$ to make sure the constructed wavelet is 'almost' analytic,

$$\sigma\omega_0 \geqslant 6 \tag{16}$$

This lower bound of 6 just corresponds to the common selection of σ = 1, ω_0 = 6. Note that a lower bound a little smaller than 6 is also acceptable (for example σ = 1, $\omega_0 = \pi\sqrt{2/\ln 2} \approx 5.3364$, so $\sigma\omega_0 \approx 5.3364$ [21], so this bound is not mathematically strict.

Secondly, for some interested pseudo frequency f_{int} in Hz, the corresponding time width of the time-frequency box or the time-frequency atom is

$$\Delta t(f_{\text{int}}) = \frac{\sigma\omega_0}{2\sqrt{2}\pi f_{\text{int}}} \tag{17}$$

and the frequency width of the time-frequency box or the time-frequency atom is

$$\Delta\omega(f_{\text{int}}) = \frac{\sqrt{2}\pi f_{\text{int}}}{\sigma\omega_0} \tag{18}$$

then the area of the time-frequency box is $\Delta t\ (f_{int})\ x\ \Delta\omega\ (f_{int}) = 1/2$, so for the Gabor mother wavelet the lower bound of 1/2 in (4) is achieved. Eqs. (17) and (18) hold for every interested frequency f_{int} in the time-frequency plane. Since the time and frequency widths of

the time-frequency box directly correspond to the time and frequency resolutions, we can say that the overall time and frequency resolutions are adjustable from the σ and ω_0 parameters of the original mother wavelet Ψ (t) without scaling (by s) and translation (by u). If the product $\sigma\omega_0$ is fixed, the time and frequency resolutions for the interested frequency f_{int} are also 'almost' fixed. If we want higher frequency resolutions (smaller $\Delta\omega\ (f_{int})$) and lower time resolutions (bigger $\Delta t\ (f_{int})$), we can increase the value of $\sigma\omega_0$. On the contrary, If we want lower frequency resolutions (bigger $\Delta\omega\ (f_{int})$) and higher time resolutions (smaller $\Delta t\ (f_{int})$), we can decrease the value of $\sigma\omega_0$, while this time we have a lower bound of 6 (or some value a little smaller than 6) for $\sigma\omega_0$ as in (16) to ensure that the mother wavelet is analytic. This adjustment of the time and frequency resolutions is global, i.e. for all the frequencies in one TFR figure, and we can't increase the frequency resolution (increasing $\sigma\omega_0$) at one frequency point and at the same moment decrease the frequency resolution (decreasing $\sigma\omega_0$) at another frequency point. In fact, this situation is just like selecting a proper window length for the STFT and the spectrogram. To achieve acceptable overall time and frequency resolutions for the analyzed signal, the initial shape (decided by the σ and ω_0 parameters for the Gabor mother wavelet) of the mother wavelet must be chosen carefully. Note that the product $\sigma\omega_0$ decides the overall resolutions instead of σ or ω_0 alone. This adjustment of the overall resolutions by the value of $\sigma\omega_0$ is applicable not only to the WT and the corresponding scalogram, but also to the reassigned scalogram, because the reassigned version is based on the scalogram. This is also true for the squeezed WT to be introduced in the next section.

Besides the fact that the overall resolutions are decided by the value of $\sigma\omega_0$, we can prove further that if $\sigma\omega_0$ is fixed, then the WT (and the derived scalogram) will be identical for various specific values of σ and ω_0. This is also true for the reassigned scalogram. The proofs are omitted here for simplicity.

The reason of including the detailed explanation of the underlying analytic wavelet transform and the overall resolutions controlled by the value of $\sigma\omega_0$ is that in some earlier investigations

of the wavelet transform as used in the analysis of the guided wave signals (as in [14]), it was believed that the wavelet transform was not acceptable because of poor resolutions, failing to perceive that in fact the resolutions are adjustable as explained above.

4. The squeezed wavelet transform

The idea of squeezing starts from the analysis of a pure harmonic signal,

$$x(t) = A\cos(\omega t) \tag{19}$$

with ω as a parameter, and its wavelet transform calculated in the frequency domain is

$$\mathrm{WT}_x^{\psi}(u,s) = \frac{A}{2}\sqrt{s}\Psi^*(s\omega)\mathrm{e}^{\mathrm{j}\omega u} \tag{20}$$

If the Fourier transform of the mother wavelet W has a compact support and is concentrated at a positive center frequency ω_0 (for example, an analytic wavelet), then the interval of the support and the center frequency are scaled by the parameter ω in (20). Note that s is now the independent variable. On the s direction, the peak of the WT appears at the scale $s = \omega_0 / \omega$ corresponding to a pseudo angular frequency of ω_0 / S, just as expected, while the energy is spread along the frequency direction on the time-frequency plane, or the s direction on the time-scale plane, instead of concentrating on the angular frequency point ω , or the scale point $s = \omega_0 / \omega$.

So this leads to the idea of reallocating the wavelet coefficients to the true instantaneous frequency, i.e. ω for the pure harmonic signal in (19). A possible solution is [21],

$$\omega(u,s) = -\mathrm{j}\frac{\frac{\partial}{\partial u}\mathrm{WT}_x^{\psi}(u,s)}{\mathrm{WT}_x^{\psi}(u,s)} \tag{21}$$

ω(u,s) is the desired instantaneous angular frequency corresponding to the original time-scale point (u,s) for the WT. Eq. (21) could be easily verified for the pure harmonic signal. Just like in the computation of the reassigned scalogram, because $WT_x^{\psi}(u,s)$ appears in the denominator, the calculation of the new frequency must be limited by a threshold value to not too small absolute WT values.

In the next step called squeezing, the WT coefficient for (u,s) on the time-scale plane should be reallocated to (u, ω(u,s)) on the time-angular frequency plane in some manner, and this reallocating should be applied to all the WT coefficients at the time instant u,

$$\mathrm{SWT}_x^{\psi}(u,\omega) = \int P\left(\mathrm{WT}_x^{\psi}(u,s),s\right)\delta(\omega(u,s)-\omega)\mathrm{d}s \qquad (22)$$

P is a function of the WT and the scale s. The δ function restricts the scale variable s to those that together with u map to ω, then the WT coefficients for these (u, s) points are transformed with P and summed (integrated) to include all their contributions to the squeezed transform for angular frequency ω. P(a,b) = $|a||b|^{-\alpha}$ was suggested in [18] for re-normalizing the fine-scale regions. For the identification of frequency components, various expressions for the function P are acceptable because we're mainly interested not in the amplitudes of the distribution but in the evolution of frequency with time.

The synchrosqueezed WT is one special case of the squeezed WT that can be used to reconstruct the original signal, with the function P defined as P(a,b) = $a.b^{-3/2}$,

$$\mathrm{SSWT}_x^{\psi}(u,\omega) = \int \mathrm{WT}_x^{\psi}(u,s)s^{-\frac{3}{2}}\delta(\omega(u,s)-\omega)\mathrm{d}s \qquad (23)$$

The reconstruction formula for the original time domain signal x(u) is

$$x(u) = \Re\left[C_{\psi}^{-1}\int_0^{\infty}\mathrm{SSWT}_x^{\psi}(u,\omega)\mathrm{d}\omega\right] \qquad (24)$$

In which $C_\psi = \frac{1}{2}\int_0^{\infty}\psi^*(\xi)\frac{d\xi}{\xi}$.

From above the ω (u, s) function is obtained for the pure harmonic signal, and the concepts of the SWT and the SSWT are given. Next it could be shown that the functions containing well separated intrinsic mode type functions (IMTs) could be characterized by synchrosqueezing. The main definitions and results from [19] are given here, without proofs.

A continuous function f is said to be of intrinsic mode type (IMT) with accuracy $\epsilon > 0$ if f(t) = A (t)$e^{j\phi(t)}$ with A and ϕ having the following properties,

$$\begin{aligned}&\inf_{t\in\mathbb{R}}\ \phi'(t)>0,\quad \sup_{t\in\mathbb{R}}\ \phi'(t)<\infty\\&|A'(t)|,\quad |\phi''(t)|\leqslant\epsilon|\phi'(t)|,\quad \forall t\in\mathbb{R}\\&\sup_{t\in\mathbb{R}}\ |\phi''(t)|<\infty.\end{aligned}\tag{25}$$

This definition shows that the function has a positive and limited instantaneous frequency, and the envelope and the instantaneous frequency change relatively more slowly compared with the phase.

A function f is said to be a superposition of, or to consist of, well separated intrinsic mode components, up to accuracy ϵ, and with separation d, if there exists a finite K, such that

$$f(t)=\sum_{k=1}^{K}f_k(t)=\sum_{k=1}^{K}A_k(t)\mathrm{e}^{\mathrm{j}\phi_k(t)}\tag{26}$$

where all the f_k are IMTs, and their phase functions ϕ_k satisfy

$$\phi_k'(t)>\phi_{k-1}'(t),\quad \frac{|\phi_k'(t)-\phi_{k-1}'(t)|}{\phi_k'(t)+\phi_{k-1}'(t)}\geqslant d,\quad \forall t\in\mathbb{R}\tag{27}$$

This condition shows that the components are well separated without intersections, and the separations of the components depend on the sum of the adjacent instantaneous frequencies.

Assume $\mathcal{A}_{\epsilon d}$ is the set of all superposition of well separated IMTs, up to accuracy ϵ and with separation d. Let f be a function in $\mathcal{A}_{\epsilon d}$ and set $\tilde{\epsilon}=\epsilon^{1/3}$. Pick a function h with $\int h(t)dt$ = 1, and pick a wavelet Ψ in Schwartz class such that its Fourier transform Ψ is supported in [1-Δ, $1+\Delta$], with Δ < d/ (1+d); set $\mathcal{R}_\phi=\sqrt{2\pi}\int\psi(\xi)\xi^{-1}d\xi$. Consider the wavelet transform $\mathrm{WT}_f^{\psi}(u,s)$ with respect to the wavelet, as well as the function $SSWT_f^{\psi}(u,\omega)$ obtained by synchrosqueezing $\mathrm{WT}_f^{\psi}(u,s)$, with threshold $\tilde{\epsilon}$ and accuracy δ, i.e.

$$\mathrm{SSWT}_f^{\psi}(u,\omega)=\int_{S_{\tilde{\epsilon}f}(u)}\mathrm{WT}_f^{\psi}(u,s)\frac{1}{\delta}h\left(\frac{\omega-\omega_f(u,s)}{\delta}\right)s^{-3/2}\,\mathrm{d}s\tag{28}$$

where $S_{\tilde{\epsilon}f}(u)=\left\{S\in\mathbb{R}_+;\ \left|WT_f^{\psi}(u,s)\right|>\tilde{\epsilon}\right\}$. Note that the expression $\frac{1}{\delta}h(\frac{\cdot}{\delta})$ (with δ as its parameter) plays the role of the function δ in(23). Then, provided ϵ (thus also $\tilde{\epsilon}$) is sufficiently small, the following hold,

$\left|WT_f^{\psi}(u,s)\right|>\tilde{\epsilon}$ only when for some k $\in$ {1, …, k}, (u,s)$\in Z_k$ = {(u,s)$|s\phi_k'(u)-1|<\Delta$},

For each k ϵ {1, …, k}, and for each pair (u,s) ϵ Z_k for which $\left|WT_f^{\psi}(u,s)\right|>\tilde{\epsilon}$ holds, we have $\left|\omega_f(u,s)-\phi_k'(u)\right| \leq \tilde{\epsilon}$

Moreover, for each k ϵ {1, …, k}, there exists a constant C such that, for any u ϵ $\mathbb{R}$

$$\left|\lim_{\delta\to 0}\left(\mathcal{R}_{\psi}^{-1}\int_{|\omega-\phi_k'(u)|<\tilde{\epsilon}} \mathrm{SSWT}_f^{\psi}(u,\omega)\mathrm{d}\omega\right)-A_k(u)\mathrm{e}^{\mathrm{j}\phi_k(u)}\right| \leqslant C\tilde{\epsilon}. \tag{29}$$

The first point of previous results shows that the WT concentrates around the scale 1 /$\phi_k'(u)$ on the time-scale plane (and around the frequency $\phi_k'(u)$ on the time-frequency plane) with 1 as the centre frequency of the mother wavelet. The second point states that the new frequency from squeezing is close to the instantaneous frequency of the component. The final one indicates that the synchrosqueezed WT is concentrated around the instantaneous frequency of the component and can be used to reconstruct the component if the WT is restricted to a narrow band around the instantaneous frequency.

For the Gabor mother wavelet, the overall time and frequency resolutions of the squeezed wavelet transform are also decided by the product $\sigma\omega_0$, since it's derived from the original WT. Furthermore, from various numerical computations, it is found that if the value of $\sigma\omega_0$ is fixed, then the synchrosqueezed wavelet transform as in (23) is identical for different combinations of σ and ω_0 values, just like the WT, the scalogram and the reassigned scalogram.

The synchrosqueezed WT is then applied to a synthesized signal s consisting of a sinusoidal frequency modulation s_1 and a quadratic frequency modulation s_2,

$$\begin{aligned} s &= s_1 + s_2, \\ s_1 &= \cos[6\pi\sin(420t) + 6000\pi t], \\ s_2 &= \cos(6\times 10^6\pi t^3 - 10.8\times 10^4\pi t^2 + 2000\pi t). \end{aligned} \tag{30}$$

The instantaneous frequencies of s_1 and s_2 in H_Z are,

$$\begin{aligned} \mathrm{IF}_{s_1} &= 1260\cos(420t) + 3000, \\ \mathrm{IF}_{s_2} &= 9\times 10^6 t^2 - 10.8\times 10^4 t + 1000. \end{aligned} \tag{31}$$

Fig. 2 shows the scalogram (2(b)) and the synchrosqueezed WT (2(d)) for the synthesized signal with an ideal TFR in Fig. 2(a), and the reassigned scalogram is also provided in Fig. 2(c) for comparison. The transforms are shown in contour plots. All the transforms are implemented in MATLAB code. A common combination of the parameters σ = 1, ω_0 = 6 is used for the non-ideal TFRs. The thresholds of the WT coefficients for the computation of the reassigned scalogram and the synchrosqueezed WT are defined in the same way for comparison,

$$\text{Thres} = \frac{\sum_{n=1}^{N} |x(n)|^2}{N} \times 10^{-3} \qquad (32)$$

with x (n) as the sample of the signal x(t) and N is the total number of the samples.

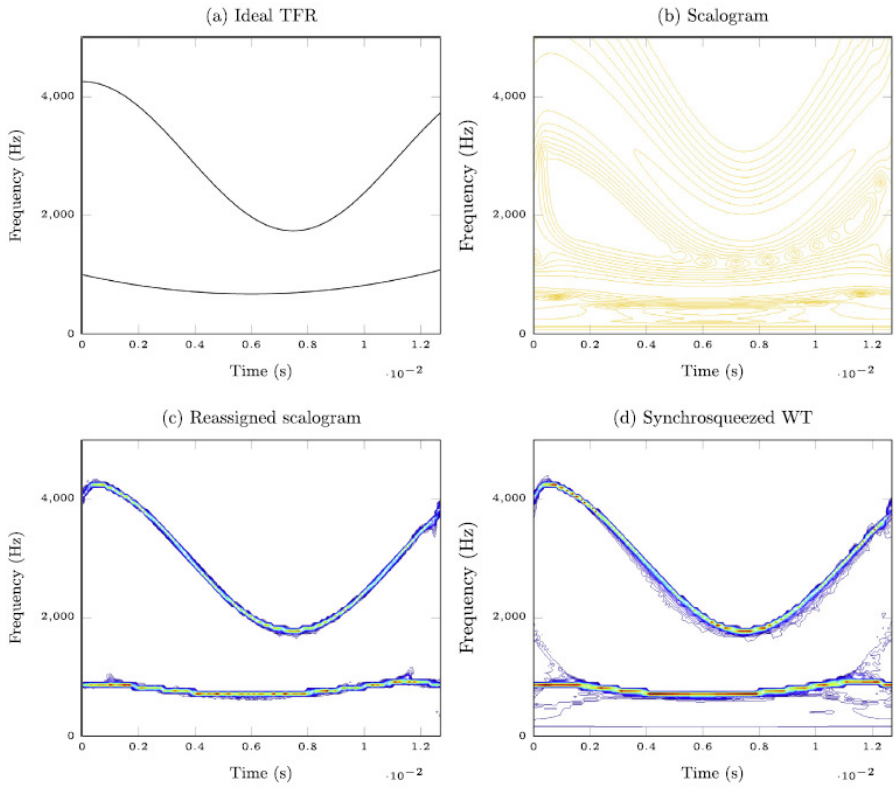

Fig.2 Ideal TFR, scalogram, reassigned scalogram and synchrosqueezed WT of a synthesized signal, with σ = 1, ω_0 = 6 for the non-ideal TFRs.

From Fig. 2, it could be observed that just like the reassigned scalogram, the synchrosqueezed WT has better time-frequency concentration compared with the original scalogram. On the

frequency direction, the reassigned scalogram has slightly better concentration than the synchrosqueezed WT. In fact, the synchrosqueezed WT is regarded as a special case of the reassignment of the wavelet transform [22]. The extra benefit of the synchrosqueezing algorithm is that it allows further signal manipulation such as reconstruction.

5. Background of Lamb waves

Lamb waves are widely used guided waves propagating in the elastic plate. Lamb waves could be decoupled into two types, the symmetric type and the antisymmetric type, according to the symmetry of the displacement components with respect to the middle plane of the plate. The dispersion equation for the symmetric modes is [23],

$$\frac{\tan(qh)}{\tan(ph)} = -\frac{4k^2pq}{\left(k^2-q^2\right)^2} \tag{33}$$

In which k is the wave number, h is half of the plate thickness, and

$$p^2 = \frac{\omega^2}{C_l^2} - k^2, \quad q^2 = \frac{\omega^2}{C_t^2} - k^2 \tag{34}$$

where ω is the angular frequency. C_l is the longitudinal bulk wave velocity, and C_t is the transverse bulk wave velocity. Similarly, the dispersion equation for the antisymmetric modes is

$$\frac{\tan(qh)}{\tan(ph)} = -\frac{\left(k^2-q^2\right)^2}{4k^2pq} \tag{35}$$

,

The dispersion equations of Lamb waves can only be solved using numerical methods. With phase velocity defined as Cp =ω/k, the results are plotted in the frequency - phase velocity plane as the phase velocity dispersion curves. The symmetric modes are often labeled as the Sn modes with n =0; 1; 2; . . ., and the antisymmetric modes are labeled as the An modes.

Group velocity (defined as Cg = dω/dk) can be calculated from the phase velocity, so from the phase velocity dispersion curves, we can obtain the group velocity dispersion curves. Group velocity corresponds to the speed of the energy propagation, so in guided wave applications we normally observe wave packets traveling with some group velocity. After proper conversion, the group velocity dispersion curves will be drawn on the time-frequency representation for easy recognition of the Lamb wave modes.

Fig. 3 shows the dispersion curves for Lamb waves propagating in a steel plate with the thickness d =0:001 m. The material properties are as follows, Young's modulus E is 207x 10^9 Pa, Poisson's ratio $\mathcal{V}$ is 0.3, and the mass density ρ is 7800 kg/m^3. These material properties will also be used for the simulation. The dispersion curves are generated with a Matlab program developed by the authors.

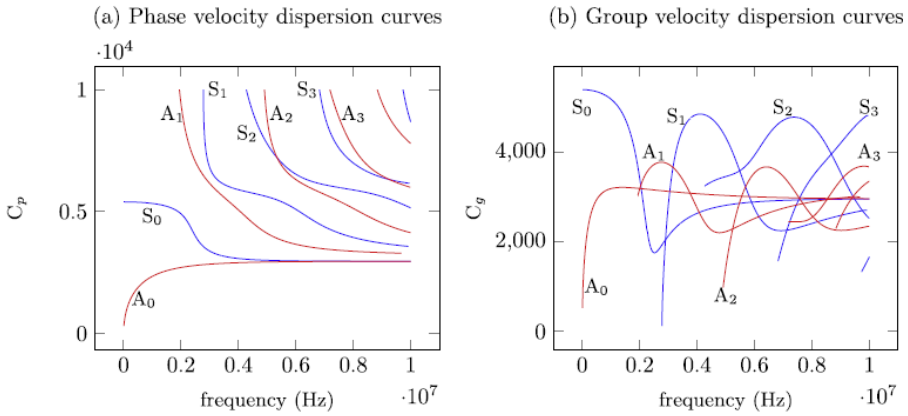

Fig.3 Dispersion curves of the Lamb waves in a steel palte, (a) phase velocity, (b) group velocity.

6. Broadband simulation of Lamb waves

For this work, the FEM package Abaqus is used to simulate the propagation of broadband Lamb waves in the steel plate free of any defect. A Python script using the Abaqus Scripting Interface is written to ease the modeling process. The 2D simulation model is depicted in Fig. 4. l= 0:2 m is the length of the plate, and d = 0:001 m is the thickness, just as in the calculation of the dispersion curves.

A plane strain Quad element with the code name of CPE4R is used as the type of these elements. The sizes of the elements in the x direction (l_{ex}) and the y direction (l_{ey}) must be chosen carefully to ensure sufficient accuracy of the simulation. l_{ey} should be small enough to make sure the number of the elements in the y direction is big enough to describe the wave

structures, i.e. the distributions of the displacement, stress or any other physical variable along the thickness of the plate waveguide, accurately. 50 is adopted as the element number in the y direction for the simulation. l_{ex} must also be small enough to ensure that there exists a sufficient number of elements in one wave length of the Lamb waves, which means that if $\lambda = Cp/f$ is the wave length and

$$\frac{\lambda}{l_{ex}} = N \tag{36}$$

then N should be at least 10 for a good spatial resolution, and the value of 20 is recommended [24]. Unlike the normal situation where a narrowband tone burst signal is used to generate an almost pure wave mode, in this work a broadband triangle impulse of displacement boundary conditions (Fig. 4) is applied as the excitation to generate a broadband signal containing multiple modes, and every mode will also occupy a wide frequency band. The expressions for the triangle impulse and its spectrum are

$$e(t) = \begin{cases} A\left(1 - \left|\frac{2t}{\delta} - 1\right|\right) & 0 \leqslant t \leqslant \delta \\ 0 & \text{otherwise} \end{cases}, \quad E(\omega) = \frac{8A\sin^2\left(\frac{\omega\delta}{4}\right)}{\omega^2\delta} e^{-j\frac{\omega\delta}{2}} \tag{37}$$

in which A is the amplitude and δ is the time width of the impulse.

Fig.4 Numerical model used in the FEM simulation.

In Fig. 5, the spectrums of the impulses with 3 different δ values of 50, 500 and 5000 ns are depicted. Obviously, the narrower the impulse, the broader is its spectrum. The impulse and corresponding spectrum are ideal in this work because in reality the excitation and the received signal are generally filtered with the characteristics of the transmitting and receiving transducers and also limited by the instrumentation. Specially designed broadband transducers and instrumentation are possible, although probably with a bandwidth much narrower than the ideal case studied here. From the view of exploratory theoretical study, the impulse waveform applied here is still meaningful.

Firstly we consider the narrowest impulse with a time width of δ = 50 ns. As in Fig. 5, the magnitude spectrum has significant frequency components in the whole frequency range explored (0– 10 MHz).

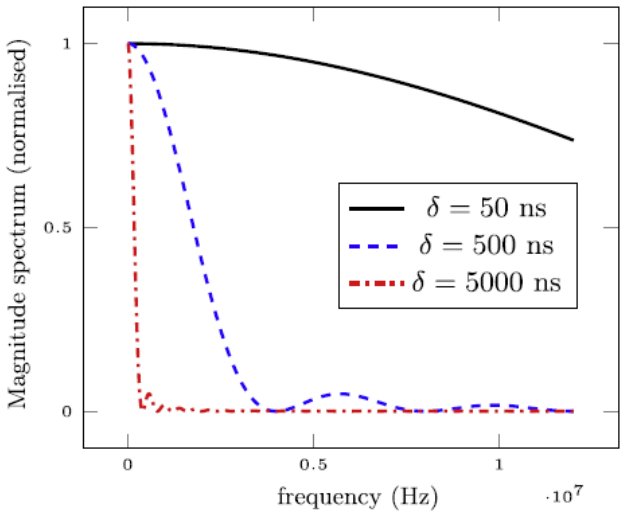

Fig.5 Normalized spectrum of triangle impulse, with δ = 50, 500 and 5000 ns.

Considering the broadband nature of the excitation signal, the wave length used to decide a proper l_{ex} should be the minimum of the wave lengths of all the excited Lamb modes contained in the signal. An estimation is used, that the minimum phase velocity is 800 m/s, and the highest frequency is 12 MHz. N is selected to be 30. This coarse estimation could be adjusted further to generate relatively accurate simulation results.

Fig. 6(a) shows the waveform of the received broadband Lamb wave signal of the displacement component υ, with an excitation impulse width of 50 ns. This signal is recorded at the coordinate ($\frac{l}{4}$, $\frac{d}{2}$) in Fig. 4. The total time of simulation is 6x 10^5 s, and this time length is selected carefully to avoid any edge reflections in the signal.

Since the impulse waveform is given as in Fig. 4 and Eq. (37), we are in a position to describe the process of converting the group velocity dispersion curves to the time-frequency plane. Because the impulse is very narrow, we can assume time 0 as the starting time instant of all the frequency components. Then a point (f, C_g) on the group velocity dispersion curves plane could be converted to the corresponding point (t, f) on the time-frequency plane

where

$$t = \frac{distance}{C_g}, \quad distance = \frac{l}{4} \tag{38}$$

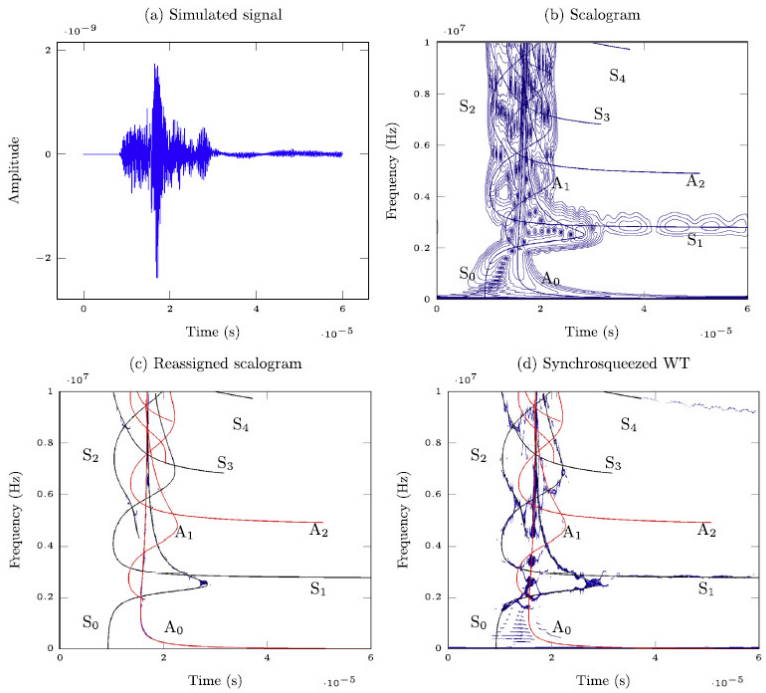

Fig.6 The simulated broadband Lamb wave signal and its scalogram, reassigned scalogram and synchrosqueezed WT, impulse width 50ns

7. Application of the squeezed wavelet transform to Lamb wave signal analysis

Fig. 6 shows the scalogram (6(b)), the reassigned scalogram (6 (c)) and the synchrosqueezed WT (6(d)) for the simulated broadband Lamb wave signal (6(a)). The combination of parameters for the Gabor mother wavelet is σ = 1, ω_0 = 11. The selection of the parameters is accomplished through traversing the ω_0 parameter (integer only) with fixed σ = 1. The traversing is coarse initially then finer, until the performance of the transform is optimum in the sense that the modes are well separated and the interferences are minimal globally. Note the traversing is only applied for the ω_0 parameter. Just as described above, the scalogram, its reassigned version and the synchrosqueezed WT all have $\sigma\omega_0$ as their parameter, so for a fixed value of $\sigma\omega_0$, different combinations of σ and ω_0 parameters will lead to identical results, then the traversing of one parameter (ω_0) is enough.

Also note that the converted group velocity dispersion curves of different wave modes intersect with each other in the time-frequency plane, so they are not well separated as expected in the definition of the (synchro)squeezed WT, but this transform could be still used for the analysis of the broadband Lamb wave signals.

From Fig. 6, it could be observed that, just like the synthesized signal, the synchrosqueezed WT has much better time-frequency concentration than the original scalogram. While compared with the reassigned scalogram, the performance of the synchrosqueezed WT is no better. At low frequencies below $0.2\text{x}10^7$ Hz, the S_0 and A_0 modes couldn't be resolved clearly and there exist interferences between them. The performance for the low frequency region could be adjusted by a different $\sigma\omega_0$ value if necessary. For example, the A_0 mode is clearer in the low frequency region for the combination of $\sigma = 1$, $\omega_0 = 6$. From Fig. 6(d), the advantage of the synchrosqueezed WT is that energy for the time later than $3\text{x}10^{-5}$ s could be observed for the S_1 and S_4 modes, while these are missing in the reassigned scalogram.

Similar simulation and time-frequency processing were also done for the impulse width of $\delta =$ 500 ns, as in Fig. 7. Obviously the frequency components are now concentrated at lower frequency range, compared with the results in Fig. 6. Through careful investigation, it could be observed that the converted group velocity curves present a small offset, because the evaluation of the propagation time duration (t in Eq. (38)) is not as accurate now, considering that the impulse width is bigger.

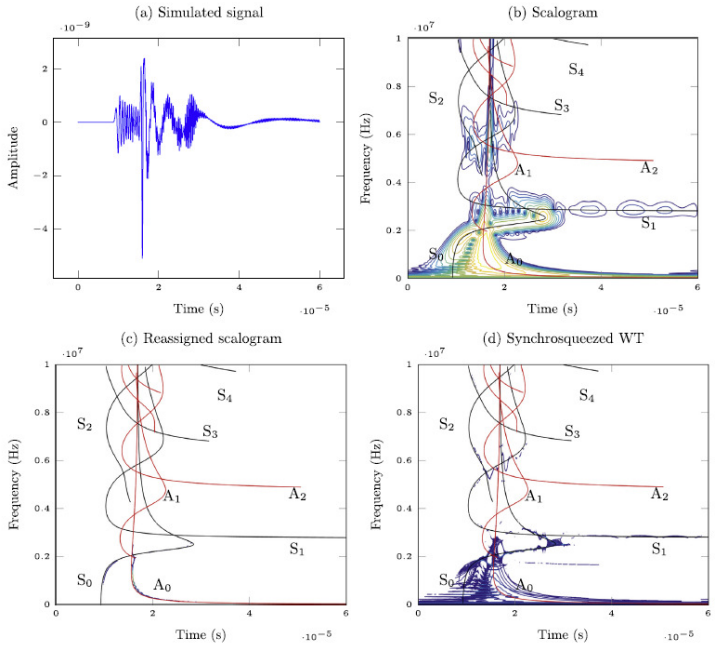

Fig.7 The simulated broadband Lamb wave signal and its scalogram, reassigned scalogram and synchrosqueezed WT, impulse width 500ns

From these observations, the synchrosqueezed WT can be used as an alternative time-frequency tool for the analysis and mode identification of guided wave signals. Even though the overall performance of the squeezed wavelet transform is no better than that of the reassigned scalogram, the synchrosqueezed WT has the additional benefit that it permits reconstruction of the original signal or its components. This advantage over the reassigned TFRs will be helpful in the detailed analysis of a broadband system. The exploration of synchrosqueezed WT-based guided wave modes extraction and signal or signal components reconstruction will be reserved for the future.

One final thing to note is that in all the simulations and calculations of the TFRs, the signals are noise-free. This should be acceptable with theoretical exploration of the underlying principles, since the practical experimental signal contaminated with noise can always be filtered beforehand.

8. Conclusion

Time-frequency analysis is crucial for the processing of ultrasonic guided wave signals because multiple modes often exist in the guided waves and these modes are dispersive. After a brief

review of common time-frequency representations and the postprocessing technique of the time-frequency reassignment for the linear TFRs, the analysis of an alternative TFR – the (synchro) squeezed wavelet transform - is given in this work. Specifically, an analytic Gabor wavelet constructed from the Gauss function is used. It is found that the product $\sigma\omega_0$ (not σ or ω_0 alone) decides the overall time and frequency resolutions of the transform. A proper selection of the product $\sigma\omega_0$ should help to improve the performance of the (synchro)squeezed WT, just like the scalogram and its reassigned version.

After a study of the squeezed wavelet transform, it is applied first to the analysis of a synthesized signal for verification, then on a simulated broadband Lamb wave signal. By traversing the value of the parameter ω_0 (integer only) for fixed σ = 1, the overall time and frequency resolutions can be adjusted. ω_0 =11 ($\sigma\omega_0$ = 11) seems to provide an approximately optimum selection of mother wavelet parameters, for the given Lamb wave signal. As expected, the synchrosqueezed WT could achieve much better time-frequency concentration than the original WT and the derived scalogram. Even though the performance of the low frequency region is no better than the reassigned scalogram, more information is observed for the later part of the signal. If better performance is needed for the low frequency region, the value of $\sigma\omega_0$ could be adjusted further.

Acknowledgements

This work is financially supported by the National Natural Science Foundation of China (Grant No. 51107058), Tsinghua University Initiative Scientific Research Program (Grant No. 20131089198), National Key Scientific Instrument and Equipment Development Project (Grant No. 2013YQ140505), and China Scholarship Council (Grant No. 201506215055).

References

[1] Prosser WH, Seale MD, Smith BT. Application of the pseudo Wigner-Ville distribution to the measurement of the dispersion of lamb modes in graphite/ epoxy plates. In: 8th International symposium on non-destructive characterization of materials, United States; 1997.

[2] Mallat S. A wavelet tour of signal processing – the sparse way. Elsevier Inc.; 2009.

[3] Jenot F, Ouaftouh M, Duquennoy M. Corrosion thickness gauging in plates using Lamb wave group velocity measurements. Meas Sci Technol 2001;12 (8):1287–93.

[4] Ho K, Billson D, Hutchins D. Ultrasonic Lamb wave tomography using scanned EMATs and wavelet processing. Nondestruct Test Eval 2007;22(1):19–34.

[5] Onsay T, Haddow A. Wavelet transform analysis of transient wave-propagation in a dispersive medium. J Acoust Soc Am 1994;95(3):1441–9.

[6] Sun Z, Mao Y, Jiang W. Investigation on interaction of Lamb waves and circumferential notch in pipe by means of wavelet transform. In: IEEE ultrasonics symposium; 2000.

[7] Silva M, Gouyon R, Lepoutre F. Hidden corrosion detection in aircraft aluminium structures using laser ultrasonics and wavelet transform signal analysis. Ultrasonics 2003;41(4):301–5.

[8] Hernandez-Salazar C, Baltazar A, Aranda-Sanchez J. Damage detection in multi-wire cables using continuous wavelet transform analysis of ultrasonic guided waves. In: CERMA 2009 – electronics robotics and automotive mechanics conference, Cuernavaca, Morelos, Mexico; 2009. p. 250–5.

[9] Liu Y, Li Z, Gong K. Detection of a radial crack in annular structures using guided circumferential waves and continuous wavelet transform. Mech Syst Sign Process 2012;30:157–67.

[10] Lee I-M, Han S-I, Kim H-J, Yu J-D, Min B-K, Lee J-S. Evaluation of rock bolt integrity using fourier and wavelet transforms. Tunn Undergr Sp Technol 2012;28(1):304–14.

[11] Prosser W, Seale MD, Smith BT. Time-frequency analysis of the dispersion of Lamb modes. J Acoust Soc Am 1999;105(5). 2669–2669.

[12] Auger F, Flandrin P. Improving the readability of time-frequency and timescale representations by the reassignment method. IEEE Trans Sign Process 1995;43(5):1068–89.

[13] Niethammer M, Jacobs LJ, Qu J, Jarzynski J. Time-frequency representation of Lamb waves using the reassigned spectrogram. J Acoust Soc Am 2000;107(5 pt 1):19–24.

[14] Niethammer M, Jacobs LJ, Qu J, Jarzynski J. Time-frequency representations of Lamb waves. J Acoust Soc Am 2001;109(5 I):1841–7.

[15] Benz R, Niethammer M, Hurlebaus S, Jacobs L. Localization of notches with Lamb waves. J Acoust Soc Am 2003;114(2):677–85.

[16] Zhang Y, Wang S, Huang S, Zhao W. Mode recognition of Lamb wave detecting signals in metal plate using the Hilbert-Huang transform method. J Sens Technol 2015(5):7–14.

[17] Zhang H, Sun X, Fan S. Lamb wave arrival time extraction using Hilbert-Huang transform for improved tomography image. J Donghua Univ 2009;26 (5):503–8.

[18] Daubechies I, Maes S. A nonlinear squeezing of the continuous wavelet transform based on auditory nerve models. CRC Press; 1996. p. 527–46 [chapter 20].

[19] Daubechies I, Lu J, Wu H-T. Synchrosqueezed wavelet transforms: an empirical mode decomposition-like tool. Appl Comput Harmon Anal 2011;30 (2):243–61.

[20] Flandrin P, Auger F, Chassande-Mottin E. Time-frequency reassignment: from principles to algorithms. LLC: CRC Press; 2003. p. 179–204

[21] Addison PS. The illustrated wavelet transform handbook. Institute of Physics Publishing; 2002.

[22] Auger F, Flandrin P, Lin Y-T, McLaughlin S, Meignen S, Oberlin T, et al. Timefrequency reassignment and synchrosqueezing. IEEE Sign Process Mag 2013;30(6):32–41.

[23] Rose JL. Ultrasonic waves in solid media. Cambridge University Press; 2004.

[24] Bartoli I, di Scalea F, Fateh M, Viola E. Modeling guided wave propagation with application to the long-range defect detection in railroad tracks. NDT&E Int 2005;38(5):325–34.